An atom probe tomography study of the oxide-metal interface of an oxide intrusion ahead of a crack in a polycrystalline Ni-based superalloy

Kitaguchi, Hiroto; Moody, M.P.; Li, Hangyue; Evans, Hugh; Hardy, Mark; Lozano-Perez, S.

DOI:
10.1016/j.scriptamat.2014.10.025

Document Version
Publisher's PDF, also known as Version of record

Citation for published version (Harvard):
Kitaguchi, H, Moody, MP, Li, H, Evans, H, Hardy, M & Lozano-Perez, S 2015, 'An atom probe tomography study of the oxide-metal interface of an oxide intrusion ahead of a crack in a polycrystalline Ni-based superalloy', *Scripta Materialia*, vol. 97, pp. 41-44. https://doi.org/10.1016/j.scriptamat.2014.10.025

Available online at www.sciencedirect.com

ScienceDirect

Scripta Materialia 97 (2015) 41–44

Scripta MATERIALIA

www.elsevier.com/locate/scriptamat

An atom probe tomography study of the oxide–metal interface of an oxide intrusion ahead of a crack in a polycrystalline Ni-based superalloy

H.S. Kitaguchi,[a,*] M.P. Moody,[a] H.Y. Li,[b] H.E. Evans,[b] M.C. Hardy[c] and S. Lozano-Perez[a]

[a]*Department of Materials, University of Oxford, Parks Road, Oxford OX1 3PH, UK*
[b]*School of Metallurgy and Materials, University of Birmingham, Birmingham B15 2TT, UK*
[c]*Rolls-Royce plc, PO Box 31, Derby DE24 8BJ, UK*

Received 5 May 2014; revised 19 October 2014; accepted 20 October 2014
Available online 8 November 2014

Intergranular oxide intrusions formed ahead of a crack in a Ni-based superalloy at 650 °C have been examined using three-dimensional atom probe tomography. Of two scans undertaken, a thin (~5 nm) alumina layer was observed next to the alloy substrate in one, overlaid by a chromia layer. In the second, chromia penetrated to the alloy interface. The chromia layer contained Ti in solution as well as discrete particles of TiO_2.

Keywords: Superalloys; Cracks; Oxide intrusions; High-temperature oxidation; Atom probe tomography

Polycrystalline Ni-based superalloys are used in aeroengines and land-based gas turbines for components such as turbine discs. These are exposed to oxidizing conditions and stress at operating temperatures in the range 500–700 °C and, clearly, the role of oxidation on crack propagation rates is an important aspect. It has been recognized for some time [1,2] that oxide intrusions could exist ahead of a crack tip but it is only recently [3] that these have been examined at sufficient spatial resolution that their nature and morphology could be reasonably established. This recent work [3] was performed on RR1000, a current-generation, high-strength turbine disc alloy of nominal composition (wt.%): 15Cr, 18Co, 3.0Al, 3.5Ti, 5.0Mo, 2.0Ta, 0.5Hf, balance Ni. In this recent work, focused ion beam (FIB) sections through the (intergranular) oxide intrusions were examined using transmission electron microscopy (TEM) coupled with energy-dispersive X-ray spectroscopy (EDX) analysis. The oxides across the intrusion width tended to be layered according to their thermodynamic stability which meant that the central region of the intrusion can be occupied by the less-stable (Ni,Co) oxides, whereas underlying this was a layer of chromia and/or alumina [3], but there was uncertainty over the distribution of Ti which may have been associated with either the chromia or alumina layers. It is important to understand the distribution of Ti since it can exist in Cr_2O_3 in solution up to concentrations of 18 at.% at 1000 °C [4] and affects Cr transport rates [5]. Similarly, protective oxide layers of chromia or alumina determine oxygen potentials within the intrusion [3] and its rate of growth [6]. The purpose of the present work was to obtain further insight into the element distribution within an oxide intrusion ahead of a crack, in a similar RR1000 specimen to that tested previously [3], using atom probe tomography (APT). Pulsed laser APT was used and this could provide 3-D atomic-scale resolution of site-specific features [7].

The microstructure of RR1000 examined in this study was identical to the study in Ref. [3]. The material was machined to corner crack test pieces having a square nett section of 4.5 × 4.5 mm^2. These were first subjected to tensile cyclic loading at 650 °C in air in order to initiate crack growth from a notch (~0.3 mm). The crack was then exposed at the same temperature in air for ~3 h without applied load, i.e., a stress intensity factor $K_i \approx 0$, as defined in Ref. [3], so that no crack growth occurred during this hold period. A Zeiss NVision 40 dual-beam FIB was used for the APT specimen preparation. The extracted specimens were analyzed in a CAMECA LEAP-3000HR instrument at 60 K with a pulse energy of ~0.6–0.7 nJ and a repetition rate of 200 kHz. It is reported by other authors that the oxides can be field-evaporated preferentially to the metal matrix [8] or vice versa [9], which can cause ion trajectory aberrations known as local magnification effects [10]. To mitigate such effects, the oxide–metal interface was aligned as closely as possible normal to the direction of ion evaporation. It is also known that oxygen has a tendency to field-evaporate as molecular-ion species [11]. This can cause peak overlaps in the resulting APT mass spectrum which, in certain instances, make it difficult to resolve the identity of an ion unambiguously. Hence, each mass

* Corresponding author. Tel.: +44 (0)1223 899000; e-mail: hiroto.kitaguchi@twi.co.uk

http://dx.doi.org/10.1016/j.scriptamat.2014.10.025
1359-6462/

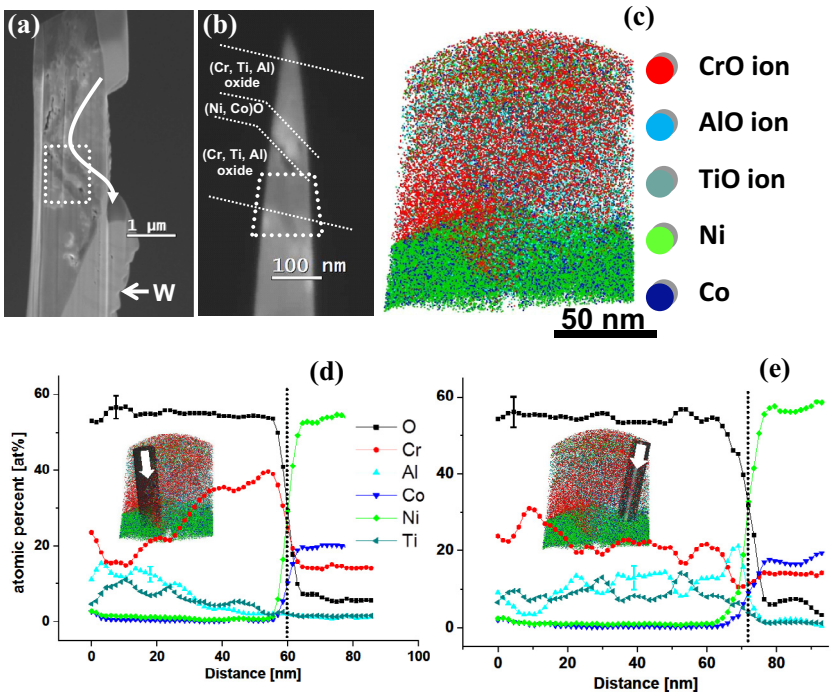

Fig. 1. SEM in-lens images of the APT specimen (a,b); APT reconstructions of the specimen (c); concentration profile through the cylindrical ROI in the reconstruction: the arrow indicates the measurement direction (d) concentration profile from another ROI as indicated in the background (e). The legend and the unit of the y axis in (e) is the same as in (d).

spectrum peak was carefully examined by a recently developed decomposition method based upon inspection of neighbouring peaks caused by isotopes and knowledge of their theoretical natural abundance [12]. The method enables more rigid quantifications for the species detected as molecular ions, i.e. oxygen. The method has an uncertainty of several per cent for the total counts of oxygen ions [12]. Hence, it was taken as an error as well as its counting statistical error and shown in one of the data points in each figure. With regard to each metallic species, the error agrees with counting statistics and an error bar is shown for one of the metallic species.

Fig. 1a and b show scanning electron microscopy (SEM) in-lens detector images of different stages in the preparation of the APT specimen, which was welded with tungsten (W) to a specimen stage, which is not included in the image. Fig. 1a shows a grain boundary with an oxide intrusion. The crack propagation direction is indicated by the white curly arrow. The tip of the oxide intrusion is located beyond the area shown in Fig. 1a, ~10 μm towards the curly arrow. The crack tip, which is defined as the furthest extent of material separation [3], is located several microns beyond the image towards the opposite direction of the arrow. In this study, an oxide morphology similar to the previous results, cf. Fig. 8 in Ref. [3], was deliberately chosen to compare results between the APT and EDX methods. Although the stress intensity factors used in the two oxides are different, the distributions of the oxygen partial pressure across the two oxide intrusions, which is an important parameter to study oxide morphologies, are considered to be comparable with each other by observing the size of the (Ni, Co)O in the centre of the oxide intrusion (see Fig. 1b). Fig 1b shows the prepared needle-shaped sample prior to the APT measurement. Analysis of the entire specimen was attempted but the (Ni,Co)O region in the central region of the intrusion fractured during the data acquisition. Only the region indicated by the trapezoidal-shaped box was analyzed successfully; however, this contains the more stable (Cr, Ti, Al) oxides of interest.

Fig. 1c shows the 3-D reconstructed specimen in which the oxide, ~70 nm thick, is the upper part of the image and the unoxidized alloy (substrate), identified by the green particles, Ni atoms, forms the lower part. Cylindrically shaped regions of interest (ROIs) were defined in order to examine the elemental concentrations across the oxide–metal interface. The diameter of the ROI was ~20 nm and this was divided lengthwise into 1.5 nm intervals. Two representative results are shown in Fig. 1d and e, where, for the sake of clarity, only the key elements are shown. In Fig. 1d, the chemistry profile starts from the top of the specimen. Very little Ni and Co was found in the oxide and the concentration of Al and Ti decreased towards the oxide–metal interface which is indicated by the broken line at 60 nm. The oxide formed in this scanned region is dominated by Cr and has a measured composition near the oxide–metal interface of $(Cr_{90}Al_{05}Ti_{05})_2O_3$. The incorporation of Al and Ti [4] into chromia is not surprising since substantial solubility is possible. No evidence of an underlying alumina layer was found in this scan. Fig. 1e shows another example of a chemistry profile taken through the same sample. Ni and Co are again essentially absent but the Cr content gradually decreases from over 30 at.% to <10 at.% at the oxide–metal interface (located at 70 nm). The Al concentration in this scan clearly increases (to >20 at.%) at the interface and indicates a layer of ~5 nm thickness. These element distributions were also confirmed in the previous investigation [3] but the improved spatial resolution of the APT technique demonstrates how thin (~5 nm) the interfacial alumina layer is. Additionally, in the scan of Fig. 1e, there is a region at ~53 nm where the Ti concentration increases at the expense of Cr and Al. The apparent composition of this feature, as taken from these

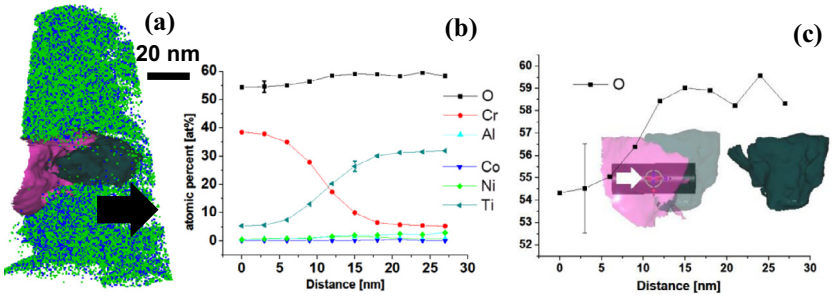

Fig. 2. APT reconstruction of specimen containing Cr-based M_2O_3 (Cr and O 75 at.% isosurface), shown by the pink isoconcentration surface, and Ti-based (Ti and O 80 at.% isosurface) oxide, shown by the dark green isoconcentration surface (a); a concentration profile across the two oxides (b); and the same concentration profile as (b) with only the oxygen profile (c), which also includes the cylindrical ROI of the concentration profile and the morphology of oxides looking head-on at the specimen tip (the left shows the isosurfaces of the two oxides and the right shows only the isosurface of Ti-based oxide to show its morphology). The legend and the unit of the y axis in (c) is the same as in (b). (For interpretation of the references to colour in this figure legend, the reader is referred to the web version of this article.)

traces, suggests a phase of the type $Cr_2Ti_{n-2}O_{2n-1}$ may be present. Work by Naoumidis et al. [4] has reported these in bulk samples from the Cr_2O_3–TiO_2 system, albeit at the higher temperature of 1000 °C.

Using a different data set, a more detailed compositional information of the Ti-rich feature mentioned above is shown in Fig. 2, which is an APT reconstruction of a specimen in which the crack is running through the middle of the specimen and the propagation direction is as indicated by the black arrow in Fig. 2a. A tip of the oxide intrusion exists a few microns away from the APT specimen on the right-hand side. The pink isoconcentration surface (isosurface) profile, which delineates the region that the total concentration of Cr and oxygen is >75 at.%, is Cr-based, leading to the conclusion that it is M_2O_3 type; the determination of the metal to oxygen stoichiometry is supported by the analyses of the previous study [3]. The dark green isosurface with the total Ti and oxygen concentration of >80 at.% highlights a Ti-based oxide. Chemical concentration profiles across the two oxides are shown in Fig. 2b and demonstrate the transition from the Cr-based to the Ti-based oxide. (Ni, Co)O was not observed in this specimen, which suggests that the oxygen partial pressure in this region is in the region of $\sim 10^{-30}$ or below [3]. This is also an indication that the region is close to the tip of the oxide intrusion [3]. The cylindrical ROI and the direction of the concentration profile are illustrated in Fig. 2c in the background, which is the identical isosurface profile as Fig. 2a but as seen from the APT detector. The concentration profile of Fig. 2c shows a profile identical to that of Fig. 2b, but with increased oxygen content, which changes from M_2O_3 (55 at.%) to Ti oxide (60 at.%). These concentrations are smaller than expected for the stoichiometric ratios for Cr_2O_3 and TiO_2, respectively, but this discrepancy can be explained by the loss in detection of oxygen ions during the APT experiment. In this study, >45% of detected events were in the form of multiple hits. This has previously been reported to lead to an underestimation of the amount of oxygen, where oxygen in a pure bulk Al_2O_3 was determined as 56.5 at.% [13]. It is concluded in this study that the measured oxygen concentration in M_2O_3 is observed to be lower than the stoichiometric ratio by 10%. TiO_2 was identified in the previous study by TEM diffraction analysis [3] which is comparable in morphology to the Ti oxide found in this study, as shown in the far right in Fig. 2c. It is concluded that the Ti-based oxide found in this study is TiO_2.

Fig. 3a shows the same APT reconstruction as Fig. 1c, but with isosurfaces for total Ti and oxygen concentrations ⩾80 at.%. The isosurfaces are all defined by the same chemical limits but the orange isosurface is a region within 20 nm of the oxide–metal interface. Fig. 3b shows the view as would be seen from the APT detector. In the background of Fig. 3c, the largest Ti-based oxide has been isolated and is highlighted with an isosurface. A corresponding proximity histogram analysis has then been undertaken to calculate the chemical concentration profile as a function of distance normal to the interface delineating the Ti-based oxide and the surrounding oxide (M_2O_3 type). The position of this interface is defined by the isosurface. Similarly Fig. 3d shows another proximity histogram for a second Ti-based oxide, the position of which is less than a few nanometers from the oxide–metal interface as indicated in the background. Oxygen clearly increases up to 60 at.% and Ti dominates the metallic elements in the oxide. The volume fraction and size of these particles become greater beyond ~50 nm from the oxide–metal interface but are

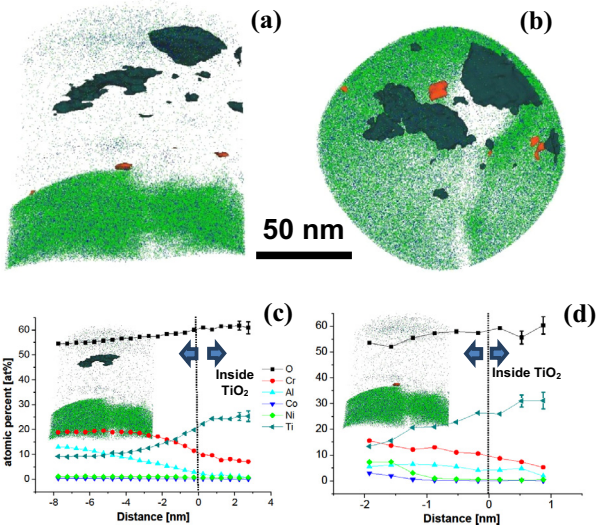

Fig. 3. Reconstructed APT tip (the same tip as in Fig. 1) with TiO_2 (Ti and O 80 at.%) isosurface side view (a) and the head-on view (b). The orange isosurface delineates TiO_2 particles close to the oxide–metal interface (<20 nm). Elemental profiles for the TiO_2 isosurface for the coarse TiO_2 (c) and fine TiO_2 close to the oxide–metal interface (d). The legend and the unit of the y axis in (d) is the same as in (c).

fewer and smaller at closer (⩽20 nm) distances. A detailed analysis of the Ti-rich oxide phases, based on 25 different particles, gives their composition as (at.%) 59.99 (2.63) O, 29.27 (3.02) Ti, 4.66 (1.65) Cr where the bracketed values are one standard deviation. No other elements were present in statistically significant quantities. The ratio of O:(Ti+Cr) concentrations is ~1.8 and again supports the view that the Ti-rich phase is essentially TiO_2 once it is recognized, as discussed above.

The APT technique has shown that a thin alumina layer (~5 nm) can be detected between chromia and the RR1000 alloy in an oxide intrusion formed ahead of a crack during a dwell period in air of 3 h at 650 °C. This layer is not always present, however, and chromia then forms in direct contact with the alloy. In each case, the chromia layer contains a dispersion of fine (<10 nm) TiO_2 particles, and this seems to be the first direct observation of such particles. Their origin remains unclear but one possibility is that the Ti solubility within the chromia layer has been exceeded and discrete particles of TiO_2 precipitate.

H.S.K. greatly appreciates the invaluable advice from Dr. Atsushi Sato, research fellow at the Department of Materials, University of Oxford. This research is supported by the Seventh Framework Programme, project reference No. 229108. The authors acknowledge support from the UK Engineering and Physical Science Research Council (EPSRC) and Rolls-Royce plc.

[1] E. Andrieu, R. Molins, H. Ghonem, A. Pineau, Mater. Sci. Eng., A 154 (1992) 21–28.
[2] D.M. Knowles, D.W. Hunt, Metall. Mater. Trans. A 33 (2002) 3165–3172.
[3] H.S. Kitaguchi, H.Y. Li, H.E. Evans, R.G. Ding, I.P. Jones, G. Baxter, P. Bowen, Acta Mater. 61 (2013) 1968–1981.
[4] A. Naoumidis, H.A. Schulze, W. Jungen, P. Lersch, J. Eur. Ceram. Soc. 7 (1991) 55–63.
[5] S. Cruchley, H.E. Evans, M.P. Taylor, M.C. Hardy, S. Stekovic, Corros. Sci. 75 (2013) 58–66.
[6] H.E. Evans, H.Y. Li, P. Bowen, Scripta Mater. 69 (2013) 179–182.
[7] K. Kruska, S. Lozano-Perez, D.W. Saxey, T. Terachi, T. Yamada, G.D.W. Smith, Corros. Sci. 63 (2012) 225–233.
[8] E.A. Marquis, Appl. Phys. Lett. 93 (2008) (1903) 181904, 181903 pp.
[9] C. Kluthe, T. Al-Kassab, R. Kirchheim, Mater. Sci. Eng., A 327 (2002) 70–75.
[10] B. Gault, M.P. Moody, J.M. Cairney, S.P. Ringer, in Springer, New York, 2012.
[11] S. Lozano-Perez, D.W. Saxey, T. Yamada, T. Terachi, Scripta Mater. 62 (2010) 855–858.
[12] H.S. Kitaguchi, S. Lozano-Perez, M.P. Moody, Ultramicroscopy 147 (2014) 51–60.
[13] E.A. Marquis, N.A. Yahya, D.J. Larson, M.K. Miller, R.I. Todd, Mater. Today 13 (2010) 34–36.